AFRL-RX-WP-TP-2010-4153

INVESTIGATION OF SELECTIVE LASER SINTERING OF ZIRCONIUM DIBORIDE PARTS (PREPRINT)

Shashwatashish Pattnaik, Ming C. Leu, and Gregory E. Hilmas

University of Missouri-Rolla

MARCH 2010

AIR FORCE RESEARCH LABORATORY
MATERIALS AND MANUFACTURING DIRECTORATE
WRIGHT-PATTERSON AIR FORCE BASE, OH 45433-7750
AIR FORCE MATERIEL COMMAND
UNITED STATES AIR FORCE

REPORT DOCUMENTATION PAGE

Form Approved
OMB No. 0704-0188

1. REPORT DATE *(DD-MM-YY)*	2. REPORT TYPE	3. DATES COVERED *(From - To)*
March 2010	Journal Article Preprint	01 March 2010 – 01 March 2010

4. TITLE AND SUBTITLE
INVESTIGATION OF SELECTIVE LASER SINTERING OF ZIRCONIUM DIBORIDE PARTS (PREPRINT)

5a. CONTRACT NUMBER
FA8650-04-C-5704

5b. GRANT NUMBER

5c. PROGRAM ELEMENT NUMBER
78011F

6. AUTHOR(S)
Shashwatashish Pattnaik, Ming C. Leu, and Gregory E. Hilmas

5d. PROJECT NUMBER
2865

5e. TASK NUMBER
25

5f. WORK UNIT NUMBER
25100000

7. PERFORMING ORGANIZATION NAME(S) AND ADDRESS(ES)
University of Missouri-Rolla
Missouri University of Science & Technology
Rolla, MO 65409-0970

8. PERFORMING ORGANIZATION REPORT NUMBER

9. SPONSORING/MONITORING AGENCY NAME(S) AND ADDRESS(ES)
Air Force Research Laboratory
Materials and Manufacturing Directorate
Wright-Patterson Air Force Base, OH 45433-7750
Air Force Materiel Command
United States Air Force

10. SPONSORING/MONITORING AGENCY ACRONYM(S)
AFRL/RXLMP

11. SPONSORING/MONITORING AGENCY REPORT NUMBER(S)
AFRL-RX-WP-TP-2010-4153

12. DISTRIBUTION/AVAILABILITY STATEMENT
Approved for public release; distribution unlimited.

13. SUPPLEMENTARY NOTES
Journal article submitted to the *Journal of Virtual and Physical Prototyping*. PAO Case Number: 88ABW-2010-0988; Clearance Date: 04 Mar 2010. Paper contains color.

This work was funded in whole or in part by Department of the Air Force Contract FA8650-04-C-5704. The U.S. Government has for itself and others acting on its behalf a paid-up, nonexclusive, irrevocable worldwide license to use, modify, reproduce, release, perform, display, or disclose the work by or on behalf of the U.S. Government.

14. ABSTRACT
This paper presents a study using the Selective Laser Sintering (SLS) process to fabricate Zirconium Diboride (ZrB_2) parts for ultra high temperature applications. Experiments were conducted to determine values of SLS process parameters (laser power, scan speed, energy density, line spacing, and layer thickness) that can be used to build ZrB_2 parts with high integrity and sharp geometrical features. A sacrificial plate with a proper number of layers (determined from experimentation) and separated from the main part, was first built in order to reduce thermal gradients. The sacrificial plate was found to assist in eliminating cracks in the bottom of the main part. The fabricated green parts then went through post processing steps including binder burnout and sintering at proper temperature schedules, to remove the binder and sinter the ZrB_2 particles. The test bars after sintering had an average relative density of 87% and an average flexural strength of 250 MPa.

15. SUBJECT TERMS
selective laser sintering (SLS), zirconium diboride (ZrB_2)

16. SECURITY CLASSIFICATION OF:			17. LIMITATION OF ABSTRACT:	18. NUMBER OF PAGES	19a. NAME OF RESPONSIBLE PERSON (Monitor)
a. REPORT	b. ABSTRACT	c. THIS PAGE			Todd J. Turner
Unclassified	Unclassified	Unclassified	SAR	38	19b. TELEPHONE NUMBER *(Include Area Code)* N/A

Standard Form 298 (Rev. 8-98)
Prescribed by ANSI Std. Z39-18

INVESTIGATION OF SELECTIVE LASER SINTERING OF ZIRCONIUM DIBORIDE PARTS

Shashwatashish Pattnaik[a], Ming C. Leu[a], Gregory E. Hilmas[b]

[a]Department of Mechanical and Aerospace Engineering, Missouri University of Science and Technology, Rolla, Missouri, USA

[b]Department of Materials Science, Missouri University of Science and Technology, Rolla, Missouri, USA

Abstract

This paper presents a study using the Selective Laser Sintering (SLS) process to fabricate Zirconium Diboride (ZrB_2) parts for ultra high temperature applications. Experiments were conducted to determine values of SLS process parameters (laser power, scan speed, energy density, line spacing, and layer thickness) that can be used to build ZrB_2 parts with high integrity and sharp geometrical features. A sacrificial plate with a proper number of layers (determined from experimentation) and separated from the main part, was first built in order to reduce thermal gradients. The sacrificial plate was found to assist in eliminating cracks in the bottom of the main part. The fabricated green parts then went through post processing steps including binder burnout and sintering at proper temperature schedules, to remove the binder and sinter the ZrB_2 particles. The test bars after sintering had an average relative density of 87% and an average flexural strength of 250 MPa.

1. Introduction

Progress in recent research and industrial applications has resulted in increased demand for ceramic part fabrication. Ceramics like ZrB_2, ZrC, HfB_2, HfC and TaC belong to the family of 'Ultra High Temperature Ceramics (UHTC)' and have found applications in the aerospace industry due to their ability to withstand extreme thermal and chemical environments [1]. The applications include, for example, hypersonic flight systems and rocket propulsion systems. Among the UHTCs, ZrB_2 has the lowest theoretical density (6.1 g/cm^3) combined with a high thermal and electrical conductivity, making its use in the aerospace industry appealing [2-5].

Fabrication of geometrically complex ceramic parts is difficult using traditional manufacturing techniques such as drilling and milling operations. This is due to the extremely brittle nature of ceramics. The high cost involved in machining of ceramics due to material wastage is another reason that reduces the desirability of using material removal methods for fabrication of complex ceramic parts.

Many Solid Freeform Fabrication (SFF) methods have been used in attempts to fabricate ceramic parts. Among these are the Fused Deposition of Ceramics (FDC) [6, 7], Chemical Liquid Deposition (CLD) [8], Selective Laser Melting (SLM) [9], Shape Deposition Manufacturing (SDM) [10, 11], 3D Printing (3DP) [12], Stereolithography (SLA) [13, 14, 15], Laminated Object Manufacturing (LOM) [16, 17] and Selective Laser Sintering (SLS) [18, 19, 20, 21]. Although these methods have been successfully implemented for freeform fabrication of ceramic parts, each has limitations on its own. Limited materials available for some of the processes, inability to fabricate complex

geometry parts, long duration to fabricate parts and difficulties in process control are some of the challenges that need to be overcome.

Other methods such as pressureless densification of ZrB_2 have been successfully used to fabricate ceramic parts of simple geometry and moderate sizes. However, due to strong covalent bonding and the low self-diffusion coefficient of ZrB_2, most researchers have used material additives such as $MoSi_2$ SiC, Si_3N_4, AlN to enhance sintering characteristics [2, 5, 22-24]. These additives improve densification by reacting with impurities, which otherwise inhibit densification and pin the growth of ZrB_2 grains. In many cases the ratio of additives to ZrB_2 has been higher than 20 vol%. Although it has been possible to achieve near full density parts with high flexural strengths [1], these methods have difficulty in producing ceramic parts with complex geometry.

Selective Laser Sintering of ZrB_2 has previously been attempted by Stucker and his research team [25, 26]. The part obtained after SLS processing was of preliminary shape and needed to be machined after debinding and sintering to obtain accurate shape. The debinded and sintered SLS-produced ZrB_2 samples were only 31% in relative density. The SLS-produced ZrB_2 EDM electrodes were infiltrated with Cu.

Another study was reported to have successfully sintered ZrB_2 part using a combination of a continuous wave and pulsed laser [27]. The continuous wave (CW) laser helped to provide heat to the part bed region to reduce the thermal stress, and the pulsed laser was used to partially melt the ZrB_2 particles. This study did not use any binder material. Instead, the smaller ZrB_2 particles melted to act as a binder for the larger ZrB_2 particles. There was no report of any mechanical properties or evidence of successful fabrication of geometrically complex parts.

The objective of the research described in the present paper was to investigate the SLS technique and to determine appropriate values of process parameters for successful fabrication of 3-dimensional ZrB_2 parts. This paper reports the results of study on fabrication of zirconium diboride parts, and the SLS parameter values were optimized by experiments. The flexural strength and density of the fabricated parts after binder burnout and sintering were measured and evaluated.

2. Discussion of process parameters and heat transfer

2.1 *Effects of process parameters*

2.1.1 *Part bed temperature*

The part bed is the central region of the SLS machine (DTM Sinterstation 2000) where the part is built. The part bed temperature is controlled by a heater underneath. The norm is to set the temperature near the glass transition temperature of the binder material, which melts to effectively fuse the particles [31]. The higher the temperature is set, the less the incident energy is required during the SLS process. The part bed temperature is also used to control the temperature gradient, thereby reducing distortion during the part sintering process [28].

2.1.2 Layer thickness

Layer thickness is a measure of the thickness of each layer during the SLS process. It is also the depth by which the part piston is lowered after the laser scanning of each layer. A stair-step effect has been observed [30] which affects the surface finish of

the side face of a fabricated part. Layer thickness plays an important role in determining the appropriate set of laser parameters, as a thicker layer requires greater incident energy to avoid delamination in fusing subsequent layers. Layer thickness also plays an important role in determining the total build time.

2.1.3 Energy density

Energy density is defined as the amount of energy input per unit area. It is dependent upon laser power, scan speed and scan spacing and is determined by the following equation [32]:

$$ED = LP / (BS \times SS) \quad \text{..... (1)}$$

where ED is the energy density, LP is the laser power, BS is the beam (or scan) speed and SS is the scan spacing. The laser power, scan speed and scan spacing need to be optimized according to the amount of input energy required to fuse the particles in the layer.

2.1.4 Effects on green part strength

The set of parameters used to fabricate a part plays a major role in influencing the green part's strength. Previous research has shown that the binder content and the energy density significantly affect the part strength [31, 33]. Higher binder content has been shown to improve the green part strength. However, higher binder content results in greater shrinkage of the part in the post processing owing to the pyrolysis of a greater amount of the binder. The other important factor that affects the strength is the incident energy density. It has been reported that the strength of the green part increases with

increase in energy density and peaks at a certain value [31]. The decrease in strength beyond the peak energy density is due to more polymer degradation at higher energy densities. The SLS parameters need to be optimized keeping these relationships in mind.

2.2 Effect of heat transfer

Since SLS is a process where the part creation revolves around heat transfer, most problems are associated with the amount of heat input and the rate of heat transfer. As the heat is applied on the top surface, the binder on the top surface melts and solidifies, resulting in contraction of the top surface and thus a change in powder density. The resultant temperature gradient perpendicular to the layered surface causes a problem of upward warping of the layer. This often results in cracking of the layer when the next layer of powder is spread and compressed by the roller. Many approaches have been taken to solve this problem [28]. In the case of metal or polymer powder, raising the part bed temperature to near the melting point of the part material can result in a reduction of temperature gradients and solve the problem of upward warping in some cases [34].

An approach introduced in the current research is the use of a sacrificial plate built from the same material as the part itself. An appropriate number of separation layers need to be provided so as to avoid sticking of the part to the sacrificial plate. The sacrificial plate would provide better conduction of heat from the top layer during laser scanning. A previous study [35] of conductivity of sintered powder compacts helps explain the phenomenon. This study reported that the effective thermal conductivity G_e of a powder compact can be calculated using the following equation:

$$G_e = G_o (1 - Ø / Ø_M)^2 \quad (2)$$

where G_o is the thermal conductivity of the monolithic material, Ø is the compact porosity and $Ø_M$ is the tap porosity. The tap porosity is the porosity of particle aggregate in equilibrium after vibration (but without compaction). It is dependent on the particle shape, size and distribution. As the tap porosity is a constant for the same particle shape, size and distribution, the effective conductivity is mainly dependent on the compact porosity, which is the porosity of the powder after compaction. A sacrificial plate effectively reduces the compact porosity of the layers underneath the main structure, thus resulting in a better conduction of heat.

3. Experiments

3.1. Materials used

The materials used for this investigation included zirconium diboride (ZrB_2, grade B, H.C. Starck, Newton, MA) with an average particle size of 3μm. The relative surface area was 1.38 m^2/g and the oxygen content was 0.9 wt%. The organic binder used was stearic acid ($C_{18}H_{36}O_2$, grade HS, Acros Organics, New Jersey), which was chosen due to its ability to easily depolymerize at higher temperatures, leaving little or no carbon residue**.** Two sintering additives used were boron carbide (B_4C, grade HS, H.C. Stark, Newton, MA) and carbon black (Black Pearls 120, Cabot corporation, Alpharetta, GA). The average particle size for the B_4C was 0.8μm with a relative surface area of 15.8 m^2/g and an oxygen content of 1.3 wt%. The sintering additives assisted with removal of the oxides from the surface of the ZrB_2 powder and increased the driving force for densification instead of grain growth.

3.2. Equipment setup

A DTM Sinterstation 2000 (Figure 1) consisting of a continuous wave CO_2 laser with an adjustable power (0 to 50W) was used for this research.. The build chamber, which is sealed during the build process to provide an inert atmosphere, can be set between room temperature and 250 ^{o}C. The 3 pistons, termed as the part piston, the left feed piston and the right feed piston, act to lower or raise the part bed, the powder in the left feed bin, and the powder in the right feed bin. The part piston is lowered by a distance equivalent to the layer thickness after each layer was scanned during the build process, while the left and right feed pistons are raised by an amount input by the user such that the roller spreads the powder to cover the whole part bed after the scanning of each successive layer. A waste bin is provided at each end of the chamber to collect any excess powder that the roller may push across the part bed.

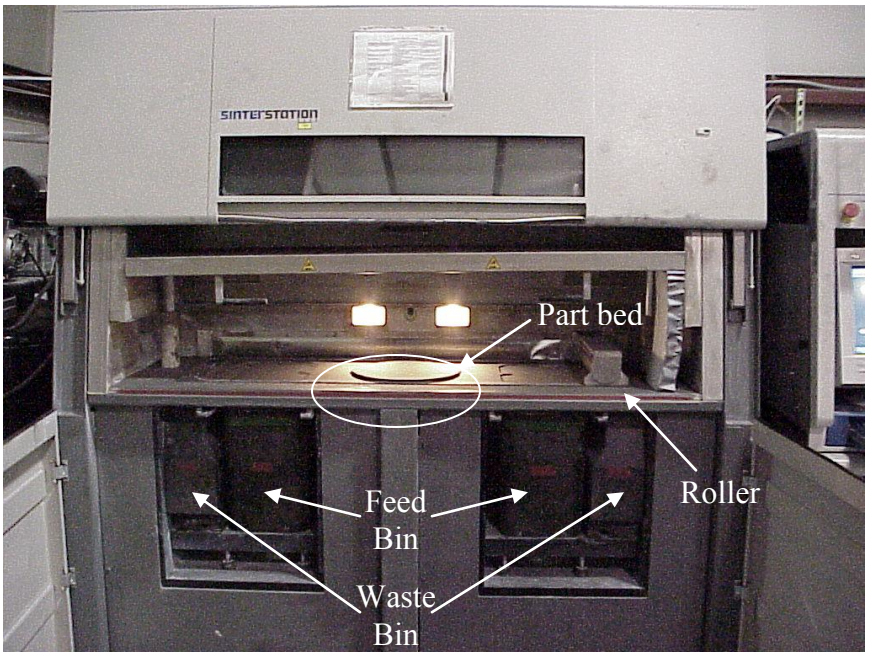

Figure 1 Sinterstation 2000

The machine has multiple parameters that can be set by the user according to the material being processed. Some of the adjustable parameters of the machine are laser power, scan speed, scan spacing, scan count, layer thickness, part piston temperature, part heater temperature, and feed bin temperature. The laser power, scan speed and scan spacing were adjusted in this study to optimize the incident energy density.

3.3. Powder preparation

Since the powder used in the SLS study consisted of ZrB_2, stearic acid, boron carbide (1 wt%) and carbon black (0.2 wt%), it needed to be a homogenous mixture to avoid irregularities in the green part formation. This was ensured by ball milling of the contents in two steps. First, zirconium diboride, boron carbide and carbon black were ball-milled together using alumina media for a period of 24 hours. The alumina media were of two sizes, 23mm and 13mm. After the first 24 hours, stearic acid was added to the mix at a volumetric ratio of 50:50 and then ball milled for another 24 hours. Due to the waxy nature of stearic acid and the heat generated due to the collision of the ceramic milling media, regular inspections were carried out to check for possible clumping.

3.4. SLS processing

Test bars and fuel injector struts as shown in Figure 2 were made by the SLS process to investigate the feasibility of fabricating ZrB_2 parts using this process. The test bars were first built for initial selection of process parameters. The temperatures considered were those of the feed bins, part bed and part heater. The fuel injector struts had at least one hole in each of the three orthogonal directions besides having curved surfaces.

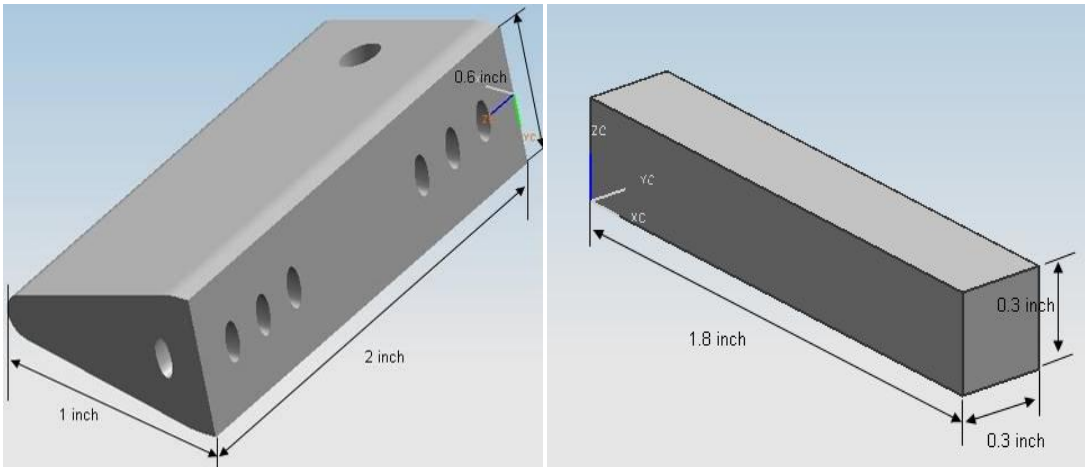

Figure 2 CAD models of fuel injector strut and test bar

The layer thickness was set at 0.0762 mm (0.003”), which is the lowest possible value that can be set in the Sinterstation 2000. This was done to attain the best surface finish and also to allow the molten binder to flow down to join the layers and help avoid delamination.

The part bed temperature was kept the same as the part piston temperature, in the range of 55 to 60 ^{o}C, to heat the powder slightly below the melting point of stearic acid, (69^{o}C). The feed bin temperature needs to be kept low enough to avoid having the binder clump (partial sintering) inside the bin, but it also has to be high enough to assist in rapid heating of the powder. It was observed that good flowability of the powder was achieved at room temperature and hence both bins were set at 26 ^{o}C. The laser power, scan speed and scan spacing were set with the help of equation (1).

The experiments performed in SLS processing consisted of the following 2 stages:

STAGE 1: This stage of tests consisted of 4 runs (RUNs 1 to 4), which were carried out to determine the appropriate energy density at which green parts could be

fabricated without delamination and were strong enough for handling. The energy densities tested were 0.068, 0.103, 0.115 and 0.172 J/mm^2 in these four runs. The corresponding parameter settings are shown in Table 1.

STAGE 2: This stage of tests consisted of 3 runs (RUNs 5 to 7), which were dedicated to addressing the issue of cracks in the bottom of the part. These 3 runs were carried out based upon the observations from the runs in STAGE 1. The parameter settings and sacrificial plates used are given in Table 1.

Table 1 Parameter settings for green part fabrication

RUN No.	Laser Power, W	Scan Speed, mm/s	Scan Spacing, mm	Energy Density, J/mm^2	No. of Separation Layers	Sacrificial Plate (cross-section size)
STAGE 1						
1	0.8	50.8	0.2286	0.068	n/a	n/a
2	1.2	50.8	0.2286	0.103	n/a	n/a
3	2	76.2	0.2286	0.115	n/a	n/a
4	3	76.2	0.2286	0.172	n/a	n/a
STAGE 2						
5	2	76.2	0.2286	0.115	5	Same as part size
6	40	1524	0.2286	0.115	5	Larger than part
7	2	76.2	0.2286	0.115	3 to 8	Larger than part

3.5. Post processing

After fabrication of green parts with the SLS machine, the successful parts underwent binder burnout, isostatic pressing and sintering. Binder burnout was carried

out in a Lindberg furnace of Type 51542-HR, where the parts were heated in varied increment rates to a temperature of 600 ^{o}C in an inert environment (90% Argon +10% Hydrogen) and held for approximately an hour to thermally decompose the binder. The binder burnout schedule was shown in Figure 3(a). Post binder burnout the specimens underwent cold isostatic pressing at a pressure of 40,000 Psi at room temperature. This was performed to reduce the porosity and the distance between particles to promote sintering in the next stage. The successful parts post isostatic pressing underwent sintering in a furnace (Hi-temp furnace, Thermal Technology Inc, Santa Rosa, California) at a temperature of 2050 ^{o}C for 2 hours. The sintering schedule followed is shown in Figure 3(b).

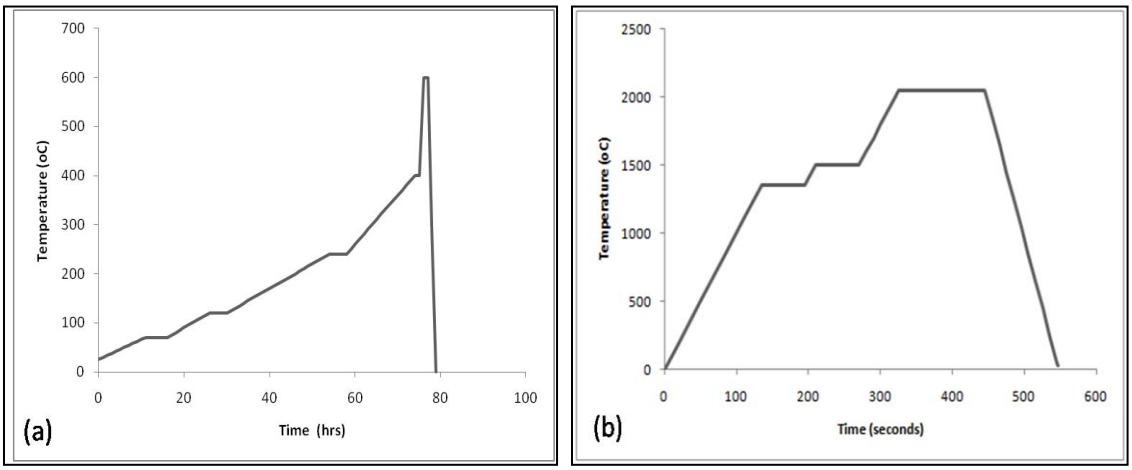

Figure 3 (a) Binder burnout schedule, (b) Sintering schedule

3.6. Characterization

The successful test bars were used to study the dimensional accuracy, density, flexural strength, surface roughness and hardness, and the microstructures were observed

to obtain pore size data. The green and sintered densities were determined by measuring the dry, saturated and suspended weight using a weighing scale (Acculab, Sartorius Group, USA) based on the Archimedes principle using water as the immersing medium. The relative density of the samples was obtained with respect to the theoretical density of ZrB_2 (6.1 g/cm^3). The flexural strength of a fully sintered specimen was measured by a 4-point bending flexural test using a universal testing machine. (Instron Corp., Model No. 5581, Norwood, MA, USA). All samples were ground to standard A bar regulations (20 x 2 x 1.5) and polished in accordance to the ASTM C1161 standards [36].

The microstructures of the specimens were observed under a Scanning Electron Microscope (S-4700, Hitachi Corp, USA). Polished, unpolished and fractured surfaces were examined to distinguish and measure the closed and open porosity in the specimens.

4. Results and discussions

4.1. Selection of SLS parameters

The Stage 1 experiments were aimed at determining an appropriate energy density for creating the melt pool. From the four runs (see Table1), RUN 3 produced parts of the highest quality. The parameter settings of RUN 3 corresponded to an energy density of 0.115 J/mm^2, which was sufficient to melt the binder and create a melt pool that could flow through the layers and bind the ZrB_2 particles together. Parts fabricated in RUN 3 demonstrated better green strength when compared to RUN 1 and RUN 2 and did not show any signs of delamination. RUN 1 did not produce any usable green parts due to insufficient energy density. RUN 2 produced parts of strength insufficient for proper handling, as only 17% of the parts survived the part breakout process without any part

breakage. Similar to RUN 3, RUN 4 was also able to produce strong parts that showed no delamination and no breakage during the part breakout process. However, parts of RUN 4 had poorer quality on the bottom surface (more material loss due to cracks on bottom surface) when compared with parts of RUN 3. In all of the runs the initial layers warped after laser scanning, which caused cracking of the initial part layers. The cracks were deeper in the case of parts fabricated at the energy density of 0.172 J/mm^2 in RUN 4 when compared with 0.115 J/mm^2 in RUN 3. The deeper cracks caused more material loss from the part bottom when blown by air during the part cleaning process. The observations from each of the 4 runs are discussed further below.

RUN 1: An energy density of 0.068 J/mm^2 was used. This was not sufficient to fabricate successful green parts. In fact, after the SLS processing the parts could be broken out only as crumbs and not as a whole part. This implies that, as a result of insufficient energy provided, the binder did not melt completely to form a melt pool sufficient to allow binding between successive layers and hence was unable to fuse the layers completely. The resulting part fabricated using this setting is shown in Figure 4(a).

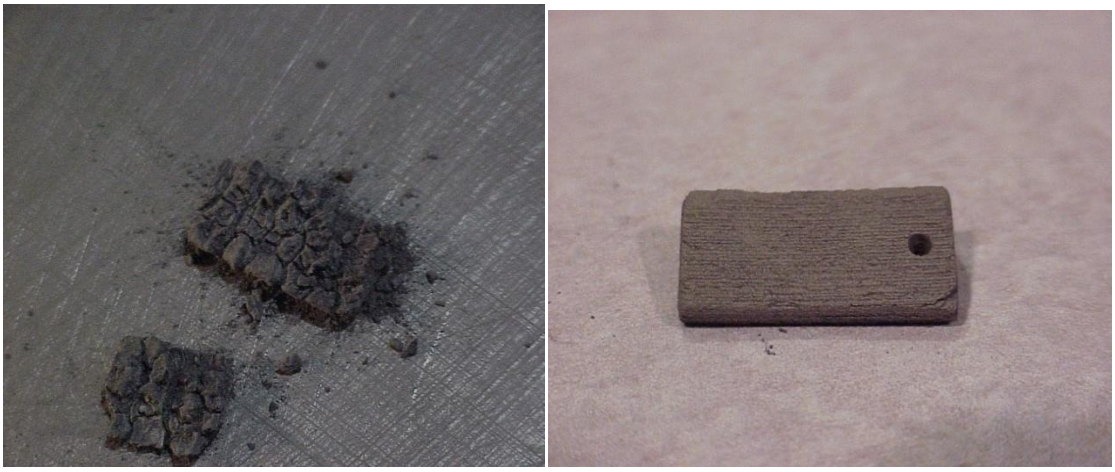

(a) (b)

Figure 4 Injector part fabricated at (a) ED=0.068 J/mm^2, (b) ED =0.103 J/mm^2

RUN 2: An energy density of 0.103 J/mm^2 was used. This energy density resulted in improved parts compared to RUN 1 even though only a few parts survived the part break-out process. The test bars fared better than the injector parts, probably due to the regular shape of the bars. Being wedge shaped, the injector struts had thinner cross sections at the beginning and end of the build. This caused varied melt pool sections and resulted in inadequate fusion between layers compared to test bar fabrication. Only 17% of the injector struts could be broken out of the part bed as complete parts as compared to 61% of test bars. All the fuel injector struts showed the problem of delamination and were too weak to be properly handled during the part break-out process. A reasonable injector part after break out is shown in Figure 4(b). All the parts had cracks in the bottom surface due to warping in the initial layers.

RUN 3: An energy density of 0.115 J/mm^2 was used. The parts fabricated had sufficient green strength for handling. As a result, all the parts survived the part break-out process. There were no signs of delamination in any of the parts. The parts did not crack or break

during the breakout process. Although the higher energy density proved to be adequate for fabricating parts with sufficient green strength for proper handling, the issue of bottom layer cracking prevailed. The cracking caused loss of material from the bottom surface of approximately 1mm in depth at the time of cleaning with an air blower.

RUN 4: An energy density of 0.172 J/mm^2 was used. This run was carried out to test if a further increase of energy density showed any significant improvement of green part quality. All the parts in this run had sufficient strength and could be broken out of the part bed. However, cracks similar to those observed in previous runs prevailed and the cracks in this run caused more loss of material than those in RUN 3 (as shown in Figure 5(a)). Hence no further runs with higher incident energy density were carried out.

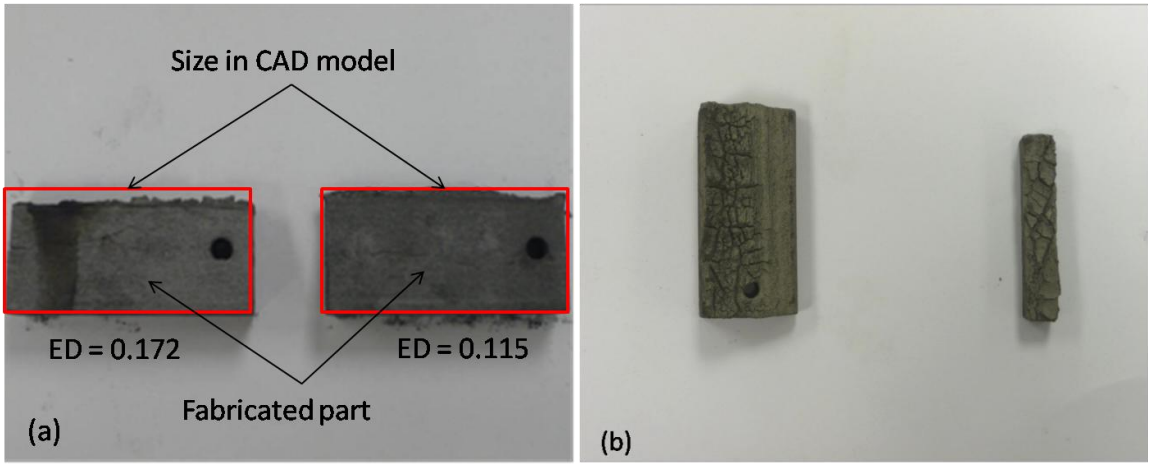

Figure 5 Some observations from fabrication of ZrB_2 parts: (a) depth of cracks at ED = 0.172 & 0.115 J/mm^2, and (b) cracked bottom surface of a fuel injector strut and a test bar

4.2. Elimination of bottom surface cracking

In all the runs performed above, the bottom surface of the parts showed cracks. These cracks were caused by deformation in the initial layers, which warped upwards after laser scanning. The warped layer then cracked when the roller applied pressure on it while spreading a new layer of powder on top of the proceeding layer. These cracks would extend until about 10-15 layers of powder had been fabricated in the SLS process. The cracks on the bottom surface of an injector strut and a test bar can be seen in Figure 5(b). The warping of the initial layers of a build is shown in Figure 6.

Figure 6 Warping of the 2nd layer after laser scanning

The warping problem was addressed by performing the following three tests:

i) A sacrificial plate (one for each part in the build) having the same X-Y dimensions as the part size was built underneath the part with 5 separation layers of loose powder between the part and the sacrificial plate. This was performed in Run 5, using the laser parameter settings developed in Run 3.

ii) A sacrificial plate covering the entire build surface area was built underneath several parts with 5 separation layers of loose powder between them. This was performed in Run 6, where the laser parameter settings were changed to increase productivity. The scan speed and the laser power were each increased by a factor of 20, keeping the energy density the same as in Run 3.

iii) One sacrificial plate covering the entire build surface area was built underneath the parts with a separation ranging from 3 to 8 layers between the part and the sacrificial plate. This was performed in Run 7. The laser parameter settings were kept the same as those in Run 3.

The parameter settings for part fabrication using a sacrificial plate are shown in Table 1. The observations made in the three runs in Stage 2 are discussed below.

RUN 5: The use of a small sacrificial plate having the same size as the built part, was not sufficient to solve the temperature gradient problem. It was unable to affect heat conduction enough to avoid warping, hence resulting in cracking in the bottom of the built part. A sacrificial plate and an injector strut built in this run are shown in Figure 7. The cracks in the bottom layers can be seen in the injector strut.

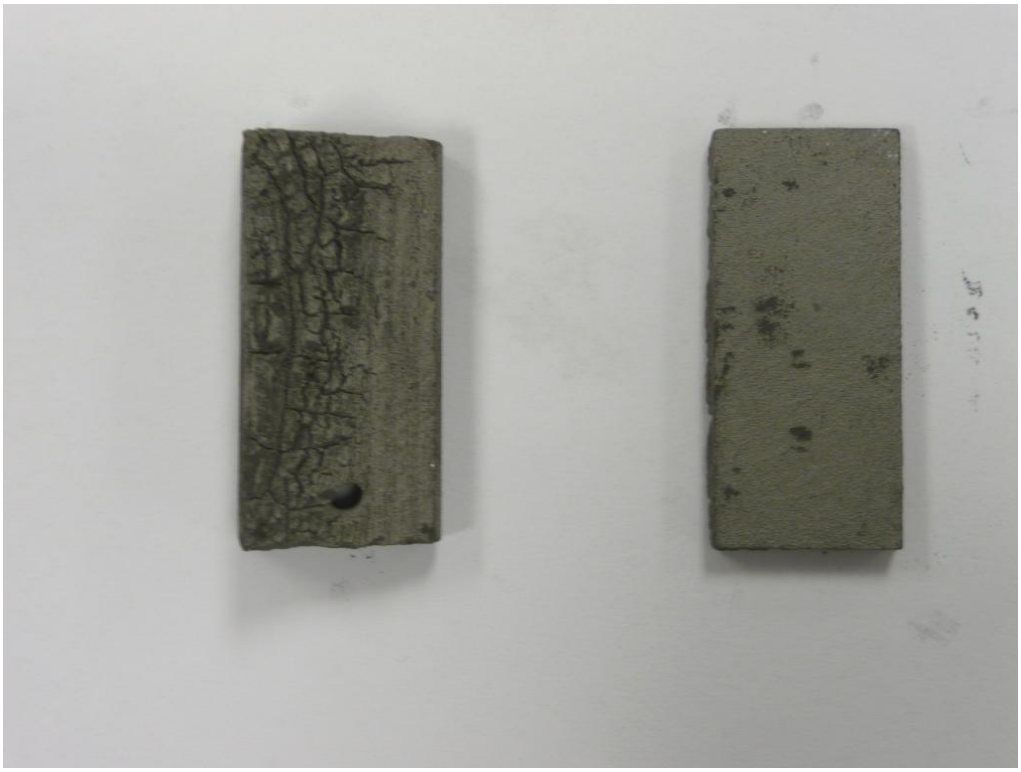

Figure 7 A fuel injector strut and a sacrificial plate built in RUN 5

RUN 6: The use of a larger sacrificial plate as shown in Figure 8(a) helped in heat conduction through the part bed but because of to the reduction of time between the layers (due to high scan speed), the melt pool increased drastically and seeped through the separation layers of loose powder and fused the sacrificial plate and the main part. Also due to the thermal stress developed in the part over the period of the build (approximately 3 hours), cracks developed throughout the part as shown in Figure 8(b).

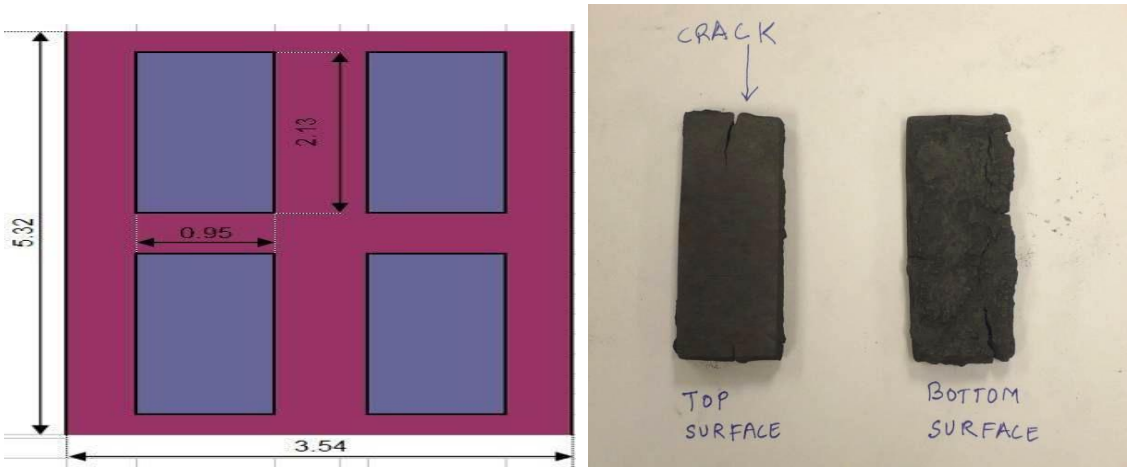

Figure 8 a) Schematic of the sacrificial plate and main parts, b) Parts fabricated in Run 6.

RUN 7: The use of a larger sacrificial plate with the laser parameters set as in Run 3 helped solve the issue of bottom layer cracking, and a part with sufficient green strength for handling and without any cracks could be successfully fabricated. The separation layers were also optimized by varying the number of separation layers in the range of 3 to 8. In the case of test bars, successful parts were fabricated with 7 and 8 layers of separation. In the case of injector struts, the successful parts were fabricated with 5 and 6 layers of separation. The difference in the separation layers for the test bars and injector struts is due to the difference in the cross section of the initial layers. The successful parts can be seen in Figure 9 and Figure 10.

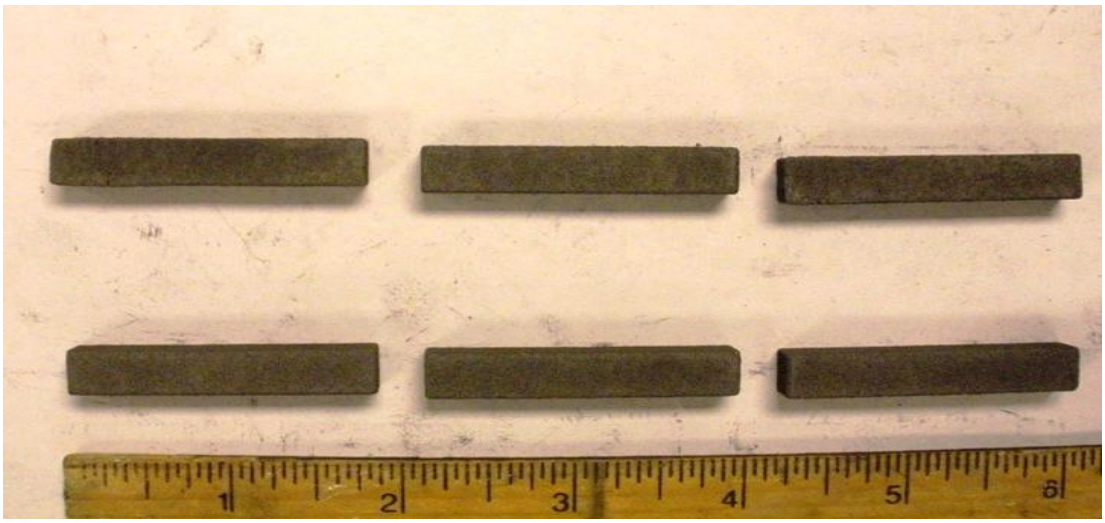

Figure 9 Green test bars fabricated with separation of 7 (bottom) and 8 (top) layers

Figure 10 Green injector parts fabricated with separation of 5 (top) and 6 (bottom) layers

The optimization of separation layers is important because a small number of separation layers would result in fusing of the main part with the sacrificial plate, whereas a large number of separation layers would result in a reduced effect of the sacrificial plate, causing cracks on the bottom surface of the main part.

Building a sacrificial plate before the main part increases the density of the powder in the region below the main part. This helps in two ways. This improves the thermal conductivity of the region as previously explained with Equation 2, which depicts that a dense material has higher thermal conductivity than a porous material. Essentially the sacrificial plate helps in the compression of the layers of loose powder spread above this plate and below the actual part, which helps in increase of heat conduction and reduction of temperature gradient. This compaction of the powder also helps physically support the sintered layer. Secondly, the sacrificial plate also helps in reducing the amount of gases below the main part, because the increase in density will cause reduction of voids and thus less space for gas. This reduces the absorptivity of the region and the temperature gradient is less due to lesser rise in temperature.

In the experiments it was observed that the depth of cracks was higher in case of ED = 0.117 J/mm^2 than in case of ED = 0.105 J/mm^2. This is due to the inability of the layers to transfer the increased heat to the surroundings, which causes higher temperature gradient and, thus build-up of larger thermal stresses.

The results of RUN 6 and RUN 7 show that the same energy density but different laser power and scan speed can produce different results. At a scan speed of 50.8 mm/s the time interval between the two consecutive laser scans of 25.4 mm long is 0.5 seconds, while in case of 1524 mm/s it is 0.017 seconds. In the case of RUN 6, the scanned layer did not get enough time to cool down and solidify sufficiently before the spreading of the next layer of powder, thus each new layer was being deposited on a partially molten layer as was observed in the experiment. Hence due to the lack of support by the previously scanned layer in fabricating a new layer the part deformed. Also the rapid heating in

RUN 6 led to development of larger thermal stresses, which contribute to part deformation and cracking.

4.3. Characterization of parts

After post-processing, the parts fabricated were evaluated for mechanical strength and density. The dimensions of the parts were measured after each stage to check for shrinkage. The microstructure of the parts was studied using SEM images.

The parts fabricated using energy density of 0.115 J/mm^2 demonstrated higher mechanical strength and density in comparison to the parts fabricated using energy density of 0.103 J/mm^2. The average shrinkage of parts fabricated using 0.115 J/mm^2 was significantly lower than those fabricated using 0.103 J/mm^2. The SEM images showed lower porosity and smaller pores in case of parts fabricated at 0.115 J/mm^2 than 0.103 J/mm^2. These results show that high energy density helps bind the particles and layers better and thus facilitates better sintering at later stage. The measured results are detailed below.

Dimensional Analysis:

The dimensions of the successful parts fabricated were measured using Mitutoyo vernier calipers. The average dimensions of the parts fabricated using energy density of 0.103 J/mm^2 is shown in Table 2. The average reductions for 10 sintered test bars fabricated in the X, Y and Z directions were 19%, 21% and 41% of the nominal dimensions, respectively. The average reductions for 10 fuel injector struts for the same settings in the X, Y and Z direction were 16%, 17% and 38% of the nominal dimensions, respectively. The dimensional changes in the X and Y directions are low as compared to that in the Z

direction. This is because the lower energy density was unable to create a melt pool that could seep downwards and sufficiently bind the particles between two layers.

Table 2 Average dimensions of parts fabricated with ED = 0.103 J/mm^2

	Dimensions (mm)			% of Nominal			Std. Deviation (mm)		
	X	Y	Z	X	Y	Z	X	Y	Z
TEST BARS									
Nominal	51.97	6.6	6.75	-	-	-	-	-	-
Green	51.93	6.83	6.55	100	103	97	0.08	0.06	0.24
Binder Burnout	49.59	6.31	4.92	95	96	73	0.23	0.10	0.36
Isostatic Press	49.56	6.29	4.87	95	95	72	0.23	0.09	0.35
Sintered	42.21	5.24	3.96	81	79	59	0.22	0.08	0.29
INJECTORS									
Nominal	25.4	12.66	7.61	-	-	-	-	-	-
Green	25.46	12.94	7.27	100	102	96	0.05	0.05	0.26
Binder Burnout	24.77	12.19	5.4	98	96	71	0.10	0.09	0.47
Sintered	21.43	10.51	4.7	84	83	61.76	0.11	0.07	0.24

The average dimensions of the parts fabricated using energy density of 0.115 J/mm^2 is shown in Table 3.The dimensional reductions in the 6 test bars fabricated were 16%, 11% and 12% of the nominal dimension in the X, Y and Z direction, respectively. The reductions in the 4 fuel injector struts fabricated were 13%, 13% and 15% of the nominal dimension in the X, Y and Z directions, respectively. The higher energy density created a sufficiently large melt pool allowing more molten binder to seep through the layer to bind more particles together and also bring them closer to each other. This is the

reason for the shrinkage in Z direction of parts fabricated in RUN 3 being lower than the shrinkage in RUN 2.

Table 3 Average dimensions of parts fabricated with ED = 0.115 J/mm^2

	Dimensions (mm)			**% of Nominal**			**Std. Deviation (mm)**		
	X	Y	Z	X	Y	Z	X	Y	Z
TEST BARS									
Nominal	45.1	7.5	7.65	-	-	-	-	-	-
Green	45.1	8.1	8.3	100	108	108	0.03	0.13	0.19
Binder Burnout	44.86	7.97	8.21	99.47	106	107	0.24	0.16	0.04
Isostatic Press	42.33	7.46	7.93	93.58	99.46	103.67	0.15	0.21	0.07
Sintered	38.01	6.65	6.72	84.27	88.67	87.84	0.47	0.10	0.14
INJECTORS									
Nominal	50.8	25.32	15.24	-	-	-	-	-	-
Green	50.9	25.82	15.69	100.19	102	103	0.21	0.30	0.12
Binder Burnout	49.97	25.62	15.33	98.37	101.2	100.60	0.37	0.22	0.16
Sintered	44.01	21.94	12.99	86.63	86.65	85.24	0.49	0.22	0.01

Density and Flexural Strength:

The relative density for the sintered test bars was measured using the Archimedes method. The parts fabricated using the energy density of 0.115 J/mm^2 had 87.1% in relative density compared to 80.3% for parts fabricated using 0.103 J/mm^2. This demonstrates better fusion of particles at higher energy density. The closer packing at higher energy density resulted in lower porosity, providing less room for shrinkage.

The density and strength data for successfully fabricated parts using the energy densities of 0.103 J/mm^2 and 0.115 J/mm^2 are shown in Table 4.The test bars fabricated

using 0.103 J/mm^2 had an average flexural strength of 195 MPa (ranging between 162 MPa to 246 MPa) for 10 test bars. The test bars fabricated using 0.115 J/mm^2 had an average flexural strength of 250 MPa (ranging between 212 MPa to 315 MPa) for 6 test bars.

Table 4 Flexural strength and density data of successfully fabricated parts

Part No.	**Flexural Strength (MPa)**		**Density (g/cc)**		**Relative Density (%)**	
	ED = 0.103 J/mm^2	ED = 0.115 J/mm^2	ED = 0.103 J/mm^2	ED = 0.115 J/mm^2	ED = 0.103 J/mm^2	ED = 0.115 J/mm^2
1	206.6	315.4	5.01	5.67	82.10	93.28
2	162.5	212.4	4.60	5.05	75.49	82.79
3	205.8	215.9	4.96	5.14	81.31	84.26
4	165.8	280.6	4.64	5.41	76.10	88.68
5	203.9	233.6	5.08	5.26	83.33	86.23
6	163.3	241.3	4.70	5.33	77.04	87.38
7	182.9	-	4.77	-	78.19	-
8	223.1	-	5.11	-	83.80	-
9	245.6	-	5.21	-	85.45	-
10	195.5	-	4.89	-	80.10	-
Average	**195.5**	**249.9**	**4.90**	**5.31**	**80.29**	**87.10**
Std. dev	**27.37**	**40.1**	**0.21**	**0.22**	**3.46**	**3.69**

SEM Study:

The microstructures studied with SEM images show that the porosity is higher in parts fabricated at lower energy density settings. Figure 11 shows the images at different magnifications of sample fractured surfaces of the test bars at the energy density settings of 0.103 J/mm^2 and 0.115 J/mm^2. It can be observed that the grain structure has larger pores and higher porosity when ED = 0.103 J/mm^2 compared with ED = 0.115 J/mm^2.

This is consistent with the observation that the density of the fabricated part at ED = 0.103 J/mm^2 is lower than that at ED = 0.115 J/mm^2.

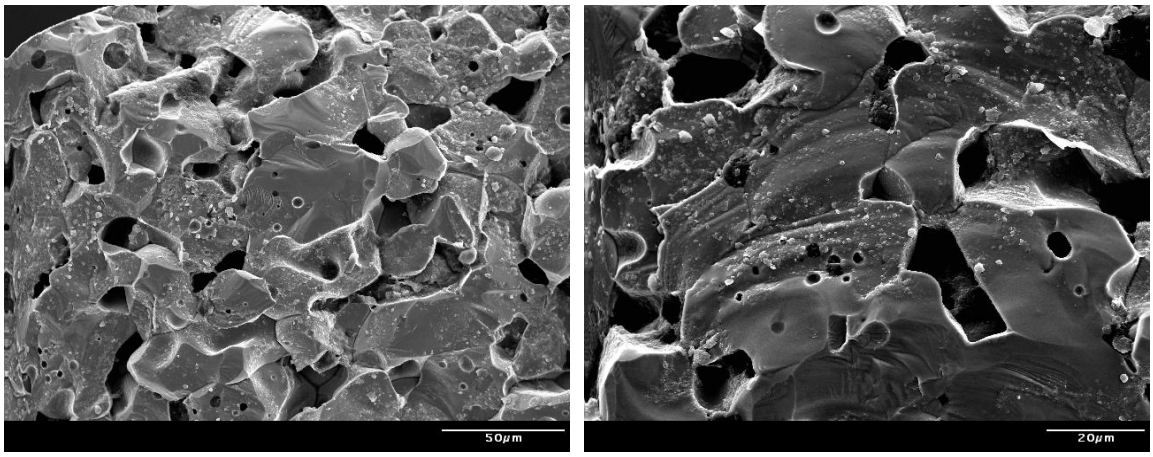

(a)

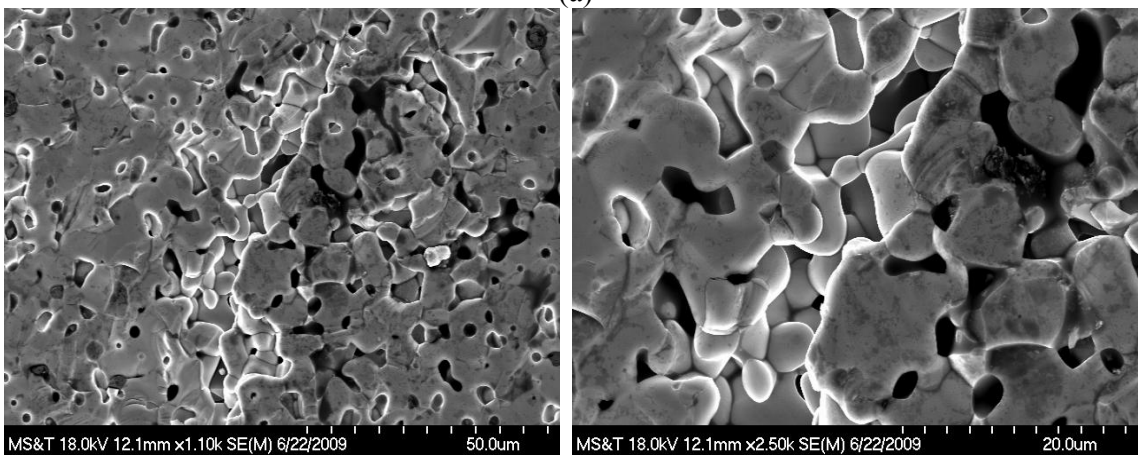

(b)

Figure 11 SEM images of fractured surfaces of test bars fabricated at (a) ED = 0.103 J/mm^2, and (b) ED =0.115 J/mm^2

5. Conclusion

The fabrication of ZrB_2 parts using the SLS process has been studied. The proper parameter settings for laser power, scan speed and scan spacing were determined

experimentally with consideration of energy density and other process parameters. The feed bin temperature, part bed temperature, and layer thickness were also determined. The use of a sacrificial plate has been shown beneficial in eliminating cracks at the bottom part surface by facilitating more uniform heat conduction and hence reduction of thermal gradient. The number of separation layers between the sacrificial plate and the main part was experimentally determined to be in the range of 5 to 8 layers in the fabrication of test bars and fuel injector struts when the layer thickness of 0.0763 mm was used. The average flexural strength of the test bars increased with increase in input energy density to 0.115 J/mm^2. The average flexural strength achieved for the fabricated parts after binder burnout and sintering was 250 MPa and the relative density achieved was 87%. The average shrinkage for the test bars fabricated was approximately 15% in each of X, Y and Z directions. The SEM images of the fracture surface were studied and it was observed that the parts fabricated at the energy density of 0.115 J/mm^2 had higher porosity than the parts fabricated with the energy density of 0.103 J/mm^2. This is consistent with the difference in the measured densities from the parts fabricated at these two energy densities.

References

1. Chamberlain, A.L., Fahrenholtz, W.G. and Hilmas, G.E., 2004. High-strength zirconium diboride-based ceramics. *Journal of American Ceramic Society*, 87 (6), 1170-1172.

2. Bellosi, A. and Monteverde, F., 2003. Fabrication and properties of zirconium diboride-based ceramics for UHT applications. *Proceedings of 4th European workshop, 'Hot structures and thermal protection systems for space vehicles'* 65-71.

3. Cutler, A., 1991. Engineering properties of borides. *Ceramics and Glasses, Engineered Materials Handbook,* 4. 787-803.

4. Shaffer, T.B., 1991. Engineering properties of carbides. *Ceramics and Glasses, Engineered Materials Handbook*, 4. 804-811.

5. Fahrenholtz, W.G., Hilmas, G.E., Chamberlain, A.L. and Zimmermann, J.W., 2004. Processing and characterization of ZrB_2 based UHTC monolithic and fibrous monolithic ceramics. *Journal of Material Science*, 39, 5951-5957.

6. Jafari, M. A., Han, W., Mohammadi, F. and Safari, A., 2000. A novel system for fused deposition of advanced multiple ceramics. *Rapid Prototyping Journal*, 6 (3), 161-175.

7. Agarwala, M. K., Jamalabad, V. R., Langrana, N. A., Safari, A., Phillip, J. W. and Danforth, S. C., 1996. Structural quality of parts processed by fused deposition. *Rapid Prototyping Journal*, 2 (4), 4-9.

8. He, Z., Zhou, J.G. and Tseng, A.A., 2000. Feasibility study of chemical liquid deposition based solid freeform fabrication. *Materials and Design*, 21 (2), 83-92.

9. Tang, Y., Fuh, J.Y.H., Loh, H.T., Wong, Y.S. and Lu, L., 2003. Direct laser sintering of silica sand. *Materials and Design*, 24 (8) 623-629.

10. Cooper, A.G., Kang, S., Kietzman, J.W., Prinz, F.B., Lombardi, J.L. and Weiss, L. 1999. Automated fabrication of complex molded parts using mold SDM. *Materials and Design*, 20 (2) 83-89.

11. Kietzman, J.W., Cooper, A.G., Weiss, L.E., Schultz, L., Lombardi, J.L. and Prinz, F.B., 1997. Layered manufacturing material issues for SDM of polymers and ceramics. *Proceedings of Solid Freeform Fabrication symposium*, 133-140.

12. Sachs, M.E., Haggerty, J.S., Cima, M.J. and Williams, P.A., 1993. Three dimensional printing techniques. *United States Patent -5,204,055.*

13. Brady, A. G. and Halloran, J. W., 1997. Stereolithography of ceramic suspensions. *Rapid Prototyping Journal*, 3 (2), 61-62.

14. Doreau, F., Chaput, C. and Chartier, T., 2000. Stereolithography for manufacturing ceramic parts. *Advanced Engineering Materials*, 2 (8), 493-496.

15. Doreau, F., Chaput, C., Chartier, T. and Loiseau, M., 2002. Stereolithography of structural complex ceramic parts. *Journal of Materials Science*, 37 (15), 3141-3147.

16. Klosterman, D.A., Chartoff, R.P., Osborne, N.R., Graves, G.A., Lightman, A., Han, G., Bezeredi, A. and Rodrigues, S., 1999. Development of a curved layer LOM process for monolithic ceramics and ceramic matrix composites. *Rapid Prototyping Journal*, 5 (2), 61-71.

17. Zhang, Y., He, X., Du, S. and Zhang, J., 2001. Al_2O_3 ceramics preparation by laminated object manufacturing. *The International Journal of Advanced Manufacturing Technology*, 17 (7), 531-534.

18. Subramanian, K., Vail, N., Barlow, J. and Marcus, H., 1995. Selective laser sintering of alumina with polymer binders. *Rapid Prototyping Journal*, 1 (2), 24-35.

19. Nelson, J.C., Vail, N., Beaman, J.J., Bourell, D.L., Barlow, J. and Marcus, H., 1995. Selective laser sintering of polymer-coated silicon carbide powders. *Industrial and Engineering Chemistry*, 34 (5), 1641-1651.

20. Bourell, D.L., Marcus, H., Barlow, J. and Beaman, J.J., 1992. Selective laser sintering of metals and ceramics. *International Journal of Powder Metallurgy*, 28 (4), 369-381.

21. Liu, Z.H., Nolte, J.J., Packard, J.I., Hilmas, G., Dogan, F. and Leu, M.C., 2007. Selective laser sintering of high-density alumina ceramic parts. *Proceedings of the 35th International MATADOR conference*, 351-354.

22. Sciti, D., Guicciardi, S., Bellosi, A. and Pezzotti, G., 2006. Properties of a pressureless-sintered ZrB_2 – $MoSi_2$ Ceramic Composite. *Journal of the American Ceramic Society*, 89 (7), 2320-2322

23. Levine S.R., Opila A. E.J., Halbig, M.C., Kiser, J.D., Singh, M. and Salem, J.A., 2002. Evaluation of ultra-high temperature ceramics for aero-propulsion use. *Journal of the European Ceramic Society*, 22 (14-15), 2757-2767.

24. Guo, S.Q., Kagawa, Y., Nishimura, T. and Tanaka, H., 2008. Pressureless sintering and physical properties of ZrB_2 based composites with $ZrSi_2$ additive. *Scripta Materialia*, 58 (7), 579-582.

25. Stucker, B.E., Bradley, W.L., Eubank, P.T., Bozkurt, B. and Norasethekkul, S., 1999. Manufacture and use of ZrB_2 /Cu or TiB_2 /Cu composite electrodes. *United States Patent – 5,933,701*.

26. Stucker, B.E., 1997. Rapid prototyping of zirconium diboride/copper EDM electrodes. Dissertation (PhD), Texas A&M University.

27. Sun, N.C. and Gupta, M.C., 2008. Laser sintering of ZrB_2. *Journal of American Ceramic Society*, 91 (5), 1729-1731.

28. Agarwala, M., Bourell, D.L., Beaman, J.J., Marcus, H. and Barlow, J., 1995. Direct selective laser sintering of metals. *Rapid Prototyping Journal*, 1 (1), 26-36.

29. Dai, K., Li, X.X. and Shaw, L.L., 2004. Comparisons between thermal modeling and experiments: effects of substrate preheating. *Rapid Prototyping Journal*, 10 (1), 24-34

30. Pham, D.T., Dimov, S. and Lacan, F., 1999. Selective laser sintering: applications and technological capabilities. *Proceedings of the Institution of Mechanical Engineers, Part B: Journal of Engineering Manufacture*, 213 (5), 435-449.

31. Gibson, I. and Shi, D., 1997. Material properties and fabrication parameters in selective laser sintering process. *Rapid Prototyping Journal*, 3 (4), 129-136.

32. Nelson, J.C., 1993. Selective Laser Sintering: A definition of the process and an empirical sintering model. Dissertation (PhD), University of Texas, Austin.

33. Badrinarayan, B. and Barlow, J.W., 1990. Effect of processing parameters in SLS of metal-polymer powders. *Proceedings of the Solid Freeform Fabrication, Austin, Texas*, 55-63.

34. Williams, J.M., Hysinger, C. and Beaman, J.J., 1992. Design of a high temperature process chamber for the selective laser sintering process. *Proceedings of the Solid Freeform Fabrication, Austin, Texas*, 110-117.

35. Montes, J.M., Rodriguez, J.A. and Herrera, E.J., 2003. Thermal and electrical conductivities of sintered powder compacts. *Powder Metallurgy*, 46 (3), 251-256.

36. ASTM International, 2008, Standard test method for flexural strength of advanced ceramics at ambient temperature, ASTM C1161-02c, West Conshohocken, Pennsylvania, USA.